American Mineralogist, Volume 81, pages 1337–1343, 1996

The structure of ordered and disordered lead feldspar ($PbAl_2Si_2O_8$)

PIERA BENNA,[1,2] MARIO TRIBAUDINO,[1] AND EMILIANO BRUNO[1,2]

[1]Dipartimento di Scienze Mineralogiche e Petrologiche, Universitá di Torino, via Valperga Caluso 35, I-10125 Turin, Italy
[2]Centro di Studi sulla Geodinamica delle Catene Collisionali (CNR), via Accademia delle Scienze 5, I-10123 Turin, Italy

ABSTRACT

The Al-Si configuration in ordered and disordered lead feldspar ($PbAl_2Si_2O_8$) has been investigated by single-crystal X-ray diffraction. Single crystals synthesized from melt and cooled from T = 1280 to 1000 °C in 1 h and then to T = 700 °C in 15 h show a completely disordered Al-Si configuration with no b-type superstructure reflections ($C2/m$, a = 8.428, b = 13.054, c = 7.174 Å, β = 115.32°; R = 5.8%). Subsequent structure refinement of a crystal hydrothermally annealed at T = 500 °C and P_{H_2O} = 2 kbar for 216 h shows an ordered Al-Si configuration ($I2/c$, a = 8.388, b = 13.067, c = 14.327 Å, β = 115.19°; R = 4.7%; $Q_{od} \approx 0.9$; 950 b reflections with $F_o \geq 4\sigma$). In the ordered lead feldspar the Pb polyhedron is significantly distorted in comparison with the Sr polyhedron in strontium feldspar. The coordination of the Pb site is reduced from sevenfold, as in strontium feldspar, to a rather irregular sixfold configuration. Such distortion could be related to the lone-pair effect in Pb^{2+}. In the disordered lead feldspar the Fourier map shows an anomalous electron-density distribution around the Pb site and consequently a split-site model for Pb was assumed in the refinement (Pb-Pb′ split = 0.557 Å).

INTRODUCTION

In feldspars and in their synthetic analogs with an Al:Si ratio of 1:1, an ordered configuration of alternating AlO_4 and SiO_4 tetrahedra is expected, leading to a unit cell with $c \approx 14$ Å. In fact, although the Al-Si configuration for anorthite is ordered, a small but significant amount of Al-Si disorder is observed at equilibrium at temperatures (T = 1530 °C) close to the melting point (Bruno et al. 1976; Benna et al. 1985; Angel et al. 1990; Carpenter et al. 1990; Carpenter 1992). Higher degrees of metastable disorder in anorthite may be obtained away from equilibrium by short annealing of anorthite glass (Carpenter 1991a, 1991b).

A highly ordered Al-Si configuration was observed in strontium feldspar (SrF) (Chiari et al. 1975), in which the macroscopic order parameter (Q_{od}), calculated according to Angel et al. (1990), was 0.78. Recently, Benna et al. (1995) found a metastable disordered Al-Si configuration (Q_{od} = 0) in strontium feldspar crystallized from melt. The evolution toward higher Al-Si ordering was followed by annealing the same sample at T = 1350 °C, eventually resulting in Q_{od} = 0.86 after 678 h. It therefore appears that, at least up to T = 1350 °C, an ordered configuration is the equilibrium state for strontium feldspar. Natural barium feldspar (celsian) is also highly ordered (Newnham and Megaw 1960), although Griffen and Ribbe (1976) showed that the observed degree of order is lower than the maximum possible.

Although the structures and Al-Si order states of anorthite, celsian, and strontium feldspar are well known, no single-crystal structure refinements exist for monoclinic lead feldspar (PbF); all that is available are cell parameters, obtained by powder diffraction (Bruno and Gazzoni 1970), and observations made from single-crystal precession photographs and IR spectra (Bruno and Facchinelli 1972). These investigations suggested that lead feldspar hydrothermally synthesized at T = 520 °C and P_{H_2O} = 1.2 kbar has a significantly ordered Al-Si configuration ($c \approx 14$ Å), whereas the same feldspar annealed at T = 1085 °C for 15 h at P = 1 bar probably has a disordered configuration ($c \approx 7$ Å). Bruno and Facchinelli (1972) suggested that these ordered and disordered Al-Si configurations are the equilibrium configurations, and that an Al-Si order-disorder transformation occurs in the subsolidus. In the present work we report the results of structure refinements of both ordered and disordered lead feldspar obtained from single-crystal X-ray–intensity data.

EXPERIMENTAL METHODS AND RESULTS

Single crystals of lead feldspar were synthesized from a stoichiometric mixture of PbO, Al_2O_3, and SiO_2, together with a slight excess of PbO to buffer for Pb volatilization and to lower the $T_{liquidus}$. The sample was melted at T = 1280 °C, quickly cooled to 1000 °C in 1 h, and then slowly cooled to 700 °C in 15 h in an electric furnace (SiC resistance, Pt-PtRh 10% thermocouple), using unsealed platinum tubes. A portion of the sample was then subjected to subsequent hydrothermal annealing at T = 500 °C and P_{H_2O} = 2 kbar for 216 h. In both cases, X-ray powder diffraction (Guinier camera, Cu$K\alpha$ radiation, λ = 1.54178 Å) revealed that lead feldspar is the only crys-

0003–004X/96/1112–1337$05.00

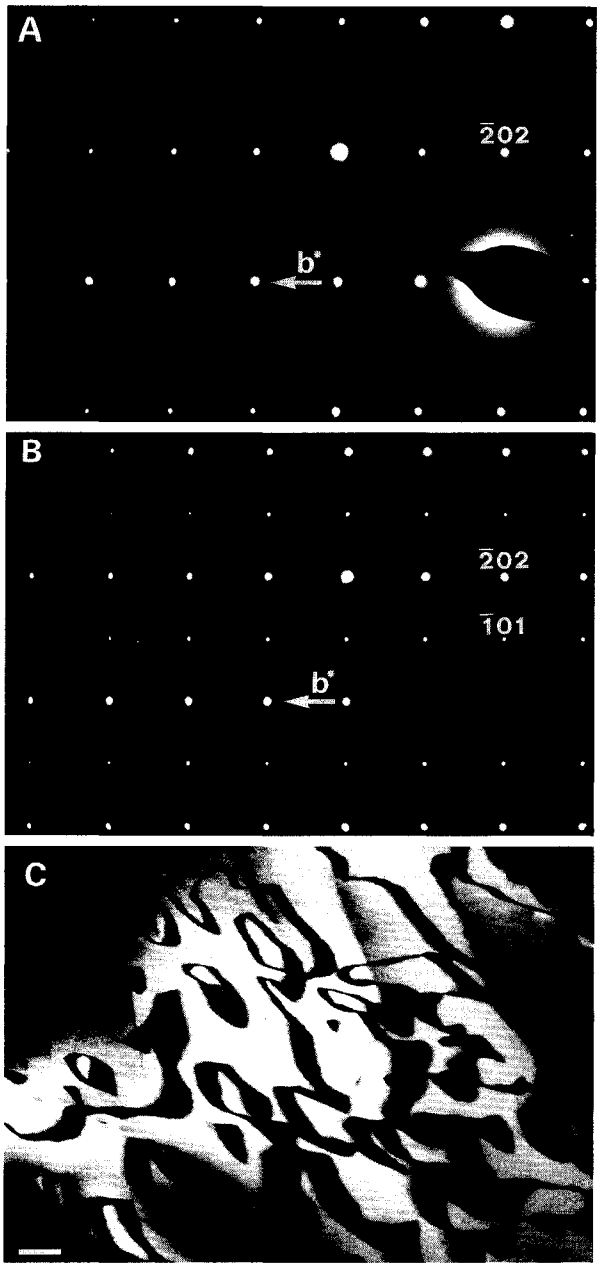

FIGURE 1. (**A**) SAD pattern of PbF_H along [101]. Only *a*-type reflections are present. (**B**) SAD pattern of PbF_L along [101]. Both *a* and *b* reflections are present. (**C**) Dark-field image of *b* antiphase domains in PbF_L; $\mathbf{g} = 21\bar{5}$; scale bar: 1000 Å.

talline phase. Crystals >100 μm in size were obtained both from the sample crystallized after melting (the disordered lead feldspar, hereafter PbF_H) and from the sample synthesized after the hydrothermal treatment (the ordered lead feldspar, hereafter PbF_L). EDS microprobe analysis performed at 15 kV on both samples did not show significant deviations from stoichiometry (PbF_H: $Pb_{1.02}Al_{1.98}Si_{2.00}O_8$; PbF_L: $Pb_{1.02}Al_{2.00}Si_{1.99}O_8$). Evidence of monoclinic symmetry was provided by the lack of splitting of high-angle X-ray powder diffraction lines, confirming previous results by Bruno and Gazzoni (1970) and Bruno and Facchinelli (1972). Transmission electron microscopy (TEM) of samples of PbF_H and PbF_L was performed using a Philips CM-12 electron microscope operating at 120 kV and equipped with double-tilt goniometer stage. The samples were crushed in an agate mortar and then deposited on a holey carbon film. Selected-area diffraction (SAD) patterns from PbF_H crystals always exhibited (according to Bown and Gay 1958) *a*-type reflections ($h + k = 2n$, $l = 2n$) (Fig. 1A), whereas *b*-type reflections ($h + k = 2n + 1$, $l = 2n + 1$) were generally absent. Extremely weak and diffuse *b* reflections were found in only a few grains. In PbF_L (Fig. 1B) both *a*- and sharp *b*-type reflections were observed in all grains, with *b* antiphase domains >1000 Å (Fig. 1C).

Single-crystal data were collected with a Siemens P4 four-circle diffractometer, using graphite-monochromatized Mo$K\alpha$ radiation (λ = 0.71073 Å) and the θ-2θ scan technique. Both *a*- and *b*-type reflections were collected. An empirical absorption correction, based on the ψ-scan method (North et al. 1968), was applied. The background and Lorentz-polarization effects were corrected using the SHELXTL-PLUS 1990 system. A weighting scheme was introduced for the final cycles of the refinements. The unit-cell parameters and the refinement data for PbF_H and PbF_L crystals are given in Table 1.

The main difference between PbF_H and PbF_L is the number and intensity of the *b*-type superstructure reflections (none with $F_o \geq 4\sigma_{F_o}$ in PbF_H and 950 in PbF_L). Therefore, the structure of PbF_H was refined in space group *C2/m*. As a starting set, the coordinates of the *C2/m* strontium feldspar from Benna et al. (1995) were used. However, anisotropic refinement gave R = 10.1% ($F_o \geq 4\sigma_{F_o}$) and nonpositive-definite values of displacement factors for T2(0). The Fourier map shows an anomalous electron-density distribution around the Pb site (the bean-like configuration of Fig. 2A); the difference Fourier shows two very strong (~10 e/Å^3) residuals. To account for these anomalous features a split-atom model for Pb was refined with two "Pb half-atoms" symmetrically positioned with respect to the mirror plane. This model yielded a significant decrease in the R value (5.8%), the disappearance of the symmetrical peaks in the difference-Fourier map, and a refined Pb-Pb′ separation of 0.557 Å, similar to that reported by Moore et al. (1989) in the synthetic feldspar $Pb_{0.77}K_{0.23}Si_{2.23}Al_{1.77}O_8$ (space group *C2/m*, Pb-Pb′ split = 0.497 Å). Splitting of the Pb site has been observed in many Pb-bearing minerals (magnetoplumbite and kentrolite, Moore et al. 1989, 1991; beudantite, Szymanski 1988; plumboferrite, Holtstam et al. 1995; lead aluminosilicate hollandite, Downs et al. 1995), with a separation between split sites similar to that found in this work.

In the PbF_L crystal, TEM and X-ray results show the presence of *a*- and *b*-type reflections, the lack of *c* ($h + k = 2n$, $l = 2n + 1$) and *d* ($h + k = 2n + 1$, $l = 2n$)

TABLE 1. Single-crystal data for PbF_H and PbF_L feldspars

	PbF_H	PbF_L
Unit-cell parameters		
a (Å)	8.428(1)	8.388(1)
b (Å)	13.054(2)	13.067(2)
c (Å)	7.174(2)	14.327(2)
β (°)	115.32(1)	115.19(1)
V (Å^3)	713.5	1421.0
Space group	$C2/m$	$I2/c$
μ (mm^{-1})	24.41	24.51
Intensity measurements		
Crystal size (mm)	0.13 × 0.10 × 0.03	0.14 × 0.09 × 0.03
Scan type technique	θ-2θ	θ-2θ
Scanning speed (°/min)	2.4–30	1–15
2θ range (°)	2–70	2–70
Index ranges	$h \pm k \pm l$	$h \pm k \pm l$
Refl. measured	7305	7292
Refl. observed $F_o \geq 4\sigma_{F_o}$	816	2269
Refl. b type	—	950
b/a	—	0.720
Refinement of the structure		
R	0.058	0.047
R_w w = $1/(\sigma^2_{F_o} + 0.0001F_o^2)$	0.054	0.042
Goodness of fit	1.69	1.46
No. of parameters	67	119

reflections, and a body-centered lattice. Therefore, a refinement in space group $I2/c$ ($c \approx 14$ Å), analogous to those of ordered strontium and barium feldspars, was performed. The coordinates of strontium feldspar (Chiari et al. 1975) were used as a starting set; the refinement converged to $R = 4.7\%$ with no significant residuals in the final difference Fourier. The Fourier map does not show any unusual electron-density distribution around the Pb site (Fig. 2B).

Atomic fractional coordinates, displacement parameters, and relevant bond lengths and angles of PbF_H and PbF_L crystals are given in Tables 2–5. Tables 6 and 7 contain the observed and calculated structure factors.[1] The Q_{od} values (Table 5 and in the text) were calculated as suggested by Angel et al. (1990) for anorthite, assuming that the effects of M cations larger than Ca and of the more open monoclinic framework on mean T-O bond lengths are negligible.

Ordered lead feldspar (PbF_L)

A distortion in the Pb polyhedron, as seen from the examination of Pb-O bond lengths (Table 5), is observed in PbF_L. In Table 8 the Pb-O distances are compared with Ba-O and Sr-O distances in barium and strontium feldspars. Most noticeable is the release of the OB(z) atom; consequently, the coordination for the Pb cation decreases to sixfold, in comparison with the coordination shown by $^{[7]}$Sr and $^{[9]}$Ba. Moreover, the Pb-OD(z) distance is significantly lower than in other $I2/c$ feldspars, and the difference between Pb-OC(z) and Pb-OC(0) is greater.

These differences can be ascribed to a polyhedral distortion, induced by a significant framework deformation, resulting from changes in the position of the O atoms, or from a displacement in the Pb position within the cavity in comparison with that of Sr and Ba in alkaline-earth feldspars. Pb in PbF_L shows a significant displacement from the c-glide plane ($y/b_{Pb} = -0.0098$), whereas Ba in celsian is on the glide plane ($y/b_{Ba} = 0$) and Sr in strontium feldspar is shifted only slightly off the plane ($y/b_{Sr} = -0.0020$). Moreover, the fractional coordinate z/c_{Pb} (0.0731) is significantly different from that of Ba ($z/c_{Ba} = 0.0653$) and Sr ($z/c_{Sr} = 0.0657$). A fictive Pb position can be calculated by linear interpolation of the coordinates between Ba and Sr. This position approximates the position that should be occupied by Pb according to a purely ionic model in which the distortion is highly reduced. It appears, therefore, that the distortion is mainly due to a shift of the Pb atom, rather than to a deformation of the framework. A similar situation is found in joesmithite when the structure of this plumbous amphibole is compared with that of hornblende (Moore et al. 1993).

Because the ionic radius of Pb^{2+} is intermediate between those of Sr and Ba (Shannon and Prewitt 1969), the observed Pb displacement and the consequent distortion of the Pb polyhedron cannot be explained simply by ionic radius considerations. In Table 8 the average Pb-O, Sr-O, and Ba-O distances for the sevenfold and ninefold coordinations are reported. The Pb-O distances are longer than Sr-O distances, according to ionic radius values reported by Shannon and Prewitt (1969). The explanation for the off-center displacement of Pb is derived from the presence of the $6s^2$ lone pair. According to this model, which has been observed in several plumbous minerals (among others hyalotekite, the structure of which is somewhat reminiscent of that of feldspars; Moore et al. 1982),

[1] A copy of Tables 6 and 7 may be ordered as Document AM-96-627 from the Business Office, Mineralogical Society of America, 1015 Eighteenth Street NW, Suite 601, Washington, DC 20036, U.S.A. Please remit $5.00 in advance for the microfiche.

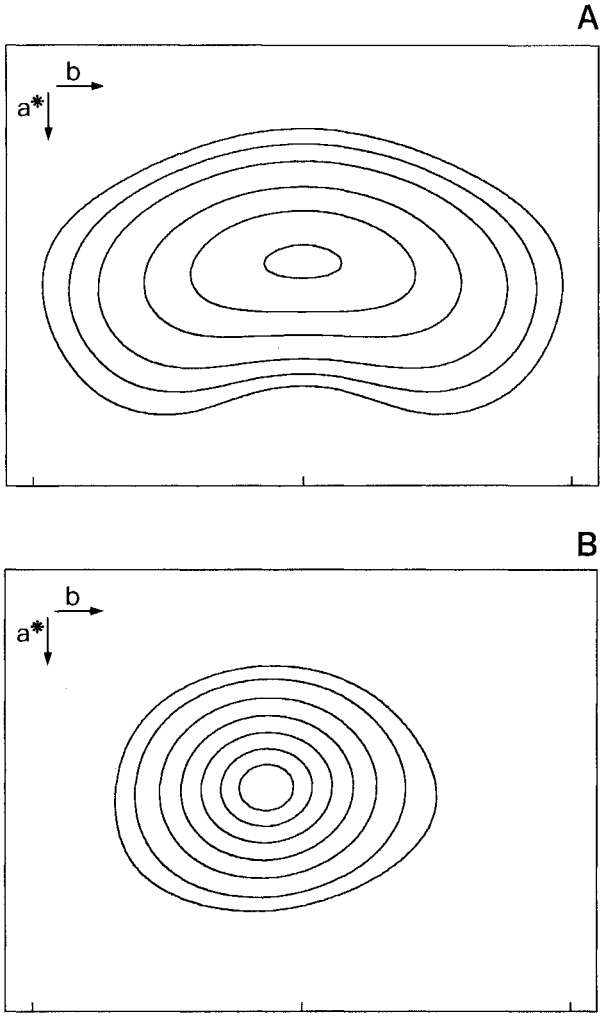

FIGURE 2. Electron-density map for the Pb site viewed along the c axis; scale: 1 Å. (**A**) PbF_H. The coordinates of the maximum are $x = 0.27$, $y = 0$, $z = 0.14$. The contours drawn correspond to 8, 20, 40, 80, 120, and 160 e/Å^3. (**B**) PbF_L. The coordinates of the maximum are $x = 0.27$, $y = -0.01$, $z = 0.07$. The contours drawn correspond to 15, 50, 120, 200, 280, 350, and 400 e/Å^3.

the presence of a lone pair of electrons within the cavity shifts the Pb atom from the centroid of the cavity toward the most underbonded atoms. This effect is prominent if asymmetry in the charge distribution within the anions in the cavity is present (Moore et al. 1993). Therefore, the bond strengths were calculated for PbF_L according to Brown and Altermatt (1985) (Table 9).

The results obtained confirm the lone-pair effect: The most saturated anion is OB(z), which is released by Pb, and the shift of Pb from the center of the cavity occurs almost along the OB(z)-OD(z) direction toward OD(z). In Figure 3B, a partial projection of the PbF_L structure on the (100) plane is shown. The distortion of the OB(0)-OB(z)-OD(0)-OD(z) quadrilateral, lying approximately on (100) (Bruno and Facchinelli 1974; Megaw 1974), is only slightly greater than in strontium feldspar (Fig. 3A), allowing the monoclinic symmetry to be maintained. On the other hand, the displacement of Pb toward OD(z) and, consequently, the release of OB(z) are evident.

A shift along the OB(m)-OD(m) direction was also observed in anorthite (Fig. 3C), in this case connected to the collapse of the framework because of the small size of the Ca cation. Therefore, in anorthite the monoclinic symmetry is forbidden by framework crumpling and by the dramatic deformation of the OB-OD quadrilateral.

Disordered lead feldspar (PbF_H)

The disordered lead feldspar (PbF_H) is characterized by the following features: (1) Al and Si are almost completely disordered at the X-ray scale, and (2) the Fourier map shows a beanlike configuration for the Pb site. These features may be explained in two ways. One possible explanation is that b antiphase domains, too small to interfere at the X-ray scale, are present. This would explain the lack of b reflections in single-crystal measurements. These b antiphase domains are formed by locally ordered $I2/c$ antiphase configurations, and Pb is locally ordered in the domains. However, if the only cause for disorder is the presence of small antiphase domains, and the structure of PbF_H is simply an average of local oppositely ordered $I2/c$ antiphase configurations, the results obtained from the refinement of PbF_H should not be significantly different from those of ordered PbF_L refined in space group $C2/m$ (without considering b reflections). Therefore, PbF_L

TABLE 2. Atomic fractional coordinates ($\times 10^4$), equivalent isotropic and anisotropic displacement coefficients (Å^2 $\times$ 10^3) in PbF_H ($C2/m$)

Site	x	y	z	U_{eq}	U_{11}	U_{22}	U_{33}	U_{12}	U_{13}	U_{23}
Pb	2749(1)	213(1)	1406(1)	41(1)	22(1)	52(1)	43(1)	16(1)	8(1)	4(1)
T1	38(3)	1793(2)	2258(4)	16(1)	18(1)	13(1)	16(1)	−5(1)	9(1)	−1(1)
T2	6932(3)	1170(2)	3455(3)	8(1)	10(1)	6(1)	8(1)	0(1)	3(1)	−0(1)
OA(1)	0	1353(8)	0	21(3)	27(5)	19(6)	15(4)	0	7(4)	0
OA(2)	6033(12)	0	2956(15)	21(4)	19(4)	12(5)	31(5)	0	10(4)	0
OB	8175(9)	1311(6)	2214(11)	27(3)	28(3)	25(5)	32(3)	0(3)	17(3)	−1(4)
OC	181(9)	3066(5)	2539(10)	24(3)	25(3)	19(4)	29(3)	−6(3)	14(3)	2(3)
OD	1905(9)	1249(6)	4010(9)	26(2)	25(3)	28(5)	16(3)	−1(3)	1(3)	−1(3)

Note: U_{eq} defined as one-third of the trace of the orthogonalized U_{ij} tensor; the anisotropic displacement exponent has the form $-2\pi^2(h^2a^{*2}U_{11} + k^2b^{*2}U_{22} + l^2c^{*2}U_{33} + 2hka^*b^*U_{12} + 2hla^*c^*U_{13} + 2klb^*c^*U_{23})$.

TABLE 3. Atomic fractional coordinates ($\times 10^4$), equivalent isotropic and anisotropic displacement coefficients ($Å^2 \times 10^3$) in PbF_L ($I2/c$)

Site	x	y	z	U_{eq}	U_{11}	U_{22}	U_{33}	U_{12}	U_{13}	U_{23}
Pb	2715(1)	−98(1)	731(1)	21(1)	9(1)	30(1)	21(1)	−2(1)	5(1)	−1(1)
T1(0)	77(3)	1755(1)	1091(1)	7(1)	7(1)	8(1)	6(1)	−2(1)	3(1)	−1(1)
T1(z)	21(3)	1797(2)	6163(1)	6(1)	6(1)	7(1)	7(1)	−2(1)	4(1)	−0(1)
T2(0)	6945(3)	1202(2)	1712(1)	6(1)	4(1)	7(1)	8(1)	1(1)	3(1)	1(1)
T2(z)	6867(3)	1137(1)	6748(1)	6(1)	5(1)	6(1)	9(1)	−1(1)	3(1)	−1(1)
OA(1)	62(7)	1336(4)	6(4)	12(1)	16(2)	15(2)	7(1)	−2(2)	5(1)	0(1)
OA(2)	5956(6)	−8(3)	1471(3)	10(1)	7(2)	4(2)	17(2)	2(2)	4(2)	2(2)
OB(0)	8280(7)	1295(4)	1055(4)	14(2)	11(2)	14(2)	23(2)	−4(2)	12(2)	−1(2)
OB(z)	8154(7)	1300(4)	6191(4)	14(2)	9(2)	19(3)	22(2)	−2(2)	13(2)	1(2)
OC(0)	178(7)	2979(4)	1217(4)	13(2)	13(2)	10(2)	18(2)	−5(2)	8(2)	−2(2)
OC(z)	182(7)	3109(4)	6328(4)	12(2)	11(2)	7(2)	18(2)	−3(2)	5(2)	−3(2)
OD(0)	1833(8)	1230(4)	1957(4)	17(2)	15(2)	21(3)	10(2)	−0(2)	0(2)	2(2)
OD(z)	2006(7)	1202(4)	7010(4)	13(2)	9(2)	14(2)	12(2)	1(2)	1(2)	1(2)

Note: U_{eq} defined as one-third of the trace of the orthogonalized U_{ij} tensor; the anisotropic displacement exponent has the form $-2\pi^2(h^2a^{*2}U_{11} + k^2b^{*2}U_{22} + l^2c^{*2}U_{33} + 2hka^*b^*U_{12} + 2hla^*c^*U_{13} + 2klb^*c^*U_{23})$.

was refined in space group $C2/m$ ($R = 4.2\%$). Displacement ellipsoids for Pb, T, and O atoms are larger than in the $I2/c$ refinement but significantly smaller than those obtained for the PbF_H (e.g., U_{eq} for Pb is 0.028 $Å^2$ in the $C2/m$ PbF_L and 0.041 $Å^2$ in the PbF_H refinement). Moreover, the displacement for Pb in PbF_H is almost twice that observed in $C2/m$ PbF_L. In conclusion, this first model does not satisfactorily account for the observed features.

The second possibility is that Pb is statically disordered in a highly disordered framework, taking up positions in each cavity determined by the local Al-Si configuration. Disorder would result not only from averaging antiphase domains but also from large disordered boundaries between the domains and from intradomain Al-Si disorder (Carpenter 1994). Intradomain Al-Si disorder in feldspars with an Al:Si ratio of 1:1 was found by Phillips et al. (1992) in anorthite. In PbF_H the intra- or interdomain Al-Si disorder induces a significant charge imbalance within the nontetrahedral site. As previously seen, the distortion of the Pb polyhedron, caused by the displacement of Pb away from the m plane, is driven by the lone-pair effect. Pb, the lone pair of which makes its position within the polyhedron extremely sensitive to slight charge im-

TABLE 4. Bond lengths (Å) and angles (°) for PbF_H ($C2/m$)

T-O distances		O-O distances		O-T-O angles
T1-OA(1)	1.706(4)	OA(1)-OB	2.642(9)	102.6(3)
T1-OB	1.680(9)	OA(1)-OC	2.847(11)	114.9(4)
T1-OC	1.672(8)	OA(1)-OD	2.631(6)	101.4(3)
T1-OD	1.694(6)	OB-OC	2.797(11)	113.1(4)
Mean	1.688	OB-OD	2.844(10)	114.9(4)
		OC-OD	2.747(10)	109.4(3)
		Mean	2.751	109.4
T2-OA(2)	1.674(5)	OA(2)-OB	2.701(13)	108.7(5)
T2-OB	1.650(10)	OA(2)-OC	2.607(7)	102.6(4)
T2-OC	1.666(7)	OA(2)-OD	2.680(9)	107.0(4)
T2-OD	1.660(6)	OB-OC	2.755(12)	112.4(4)
Mean	1.663	OB-OD	2.740(11)	111.8(4)
		OC-OD	2.786(8)	113.8(4)
		Mean	2.712	109.4

Pb-O distances*		T-O-T angles	
Pb-OA(1)	2.927(7)	T1-OA(1)-T1	140.6(7)
Pb-OA(1)	2.569(6)	T2-OA(2)-T2	131.6(6)
Pb-OA(2)	2.518(10)	T1-OB-T2	146.7(5)
Pb-OB	2.770(8)	T1-OC-T2	130.4(5)
Pb-OB	3.095(8)	T1-OD-T2	139.9(5)
Pb-OC	3.360(7)	Mean	137.8
Pb-OC	2.912(7)		
Pb-OD	2.962(8)		
Pb-OD	2.638(8)		

* The refinement was performed according to a $C2/m$ configuration for the disordered framework and according to a split-site model for Pb.

TABLE 5. Bond lengths (Å), angles (°), and Q_{od} value for PbF_L ($I2/c$)

T-O distances		O-O distances		O-T-O angles
T1(0)-OA(1)	1.643(6)	OA(1)-OB(0)	2.533(10)	102.5(3)
T1(0)-OB(0)	1.604(6)	OA(1)-OC(0)	2.736(8)	114.6(3)
T1(0)-OC(0)	1.609(5)	OA(1)-OD(0)	2.552(6)	102.9(3)
T1(0)-OD(0)	1.620(5)	OB(0)-OC(0)	2.669(8)	112.4(3)
Mean	1.619	OB(0)-OD(0)	2.698(8)	113.6(3)
		OC(0)-OD(0)	2.651(7)	110.4(3)
		Mean	2.640	109.4
T1(z)-OA(1)	1.753(6)	OA(1)-OB(z)	2.714(9)	103.2(3)
T1(z)-OB(z)	1.712(6)	OA(1)-OC(z)	2.954(7)	116.2(3)
T1(z)-OC(z)	1.727(5)	OA(1)-OD(z)	2.668(6)	98.5(3)
T1(z)-OD(z)	1.770(5)	OB(z)-OC(z)	2.869(7)	113.1(3)
Mean	1.741	OB(z)-OD(z)	2.934(7)	114.8(3)
		OC(z)-OD(z)	2.869(7)	110.2(2)
		Mean	2.835	109.3
T2(0)-OA(2)	1.751(5)	OA(2)-OB(0)	2.836(8)	108.4(3)
T2(0)-OB(0)	1.746(7)	OA(2)-OC(0)	2.718(6)	103.2(2)
T2(0)-OC(0)	1.717(5)	OA(2)-OD(0)	2.752(6)	104.1(3)
T2(0)-OD(0)	1.739(5)	OB(0)-OC(0)	2.870(9)	111.9(3)
Mean	1.738	OB(0)-OD(0)	2.890(8)	112.0(3)
		OC(0)-OD(0)	2.935(6)	116.2(3)
		Mean	2.833	109.3
T2(z)-OA(2)	1.631(4)	OA(2)-OB(z)	2.653(8)	110.0(3)
T2(z)-OB(z)	1.607(7)	OA(2)-OC(z)	2.532(6)	102.5(3)
T2(z)-OC(z)	1.615(5)	OA(2)-OD(z)	2.631(6)	108.0(3)
T2(z)-OD(z)	1.622(5)	OB(z)-OC(z)	2.696(9)	113.6(3)
Mean	1.619	OB(z)-OD(z)	2.640(8)	109.7(3)
		OC(z)-OD(z)	2.695(6)	112.7(3)
Q_{od}	0.89	Mean	2.641	109.4

Pb-O distances		T-O-T angles	
Pb-OA(1)	2.753(5)	T1(0)-OA(1)-T1(z)	140.4(4)
Pb-OA(1)	2.657(5)	T2(0)-OA(2)-T2(z)	129.5(3)
Pb-OA(2)	2.465(5)	T1(0)-OB(0)-T2(0)	145.0(3)
Pb-OB(0)	2.806(5)	T1(z)-OB(z)-T2(z)	151.2(3)
Pb-OB(z)	3.121(5)	T1(0)-OC(0)-T2(0)	131.4(3)
Pb-OC(0)	3.346(5)	T1(z)-OC(z)-T2(z)	131.4(3)
Pb-OC(z)	3.000(5)	T1(0)-OD(0)-T2(0)	140.2(4)
Pb-OD(0)	2.784(6)	T1(z)-OD(z)-T2(z)	135.6(4)
Pb-OD(z)	2.592(6)	Mean	138.1

TABLE 8. Pb-O, Sr-O, and Ba-O bond lengths (Å) for lead, strontium, and barium feldspars

	Pb	Sr	Ba
OA(1)	2.753(5)	2.624(8)	2.847(6)
OA(1)	2.657(5)	2.641(8)	2.854(6)
OA(2)	2.465(5)	2.437(5)	2.641(5)
OB(0)	2.806(5)	2.744(8)	2.924(7)
OB(z)	3.121(5)	2.853(8)	2.949(6)
OC(0)	3.346(5)	3.237(7)	3.150(7)
OC(z)	3.000(5)	3.083(8)	3.124(6)
OD(0)	2.784(6)	2.766(9)	2.916(6)
OD(z)	2.592(6)	2.744(9)	2.903(6)
⟨[6]M-O⟩	2.676	—	—
⟨[7]M-O⟩	2.722	2.687	2.862
⟨[9]M-O⟩	2.836	2.792	2.923

Note: Pb = lead feldspar (PbF_L), this work; Sr = strontium feldspar (T = 1350 °C, t = 678 h, Benna et al. 1995); Ba = celsian (Griffen and Ribbe 1976).

TABLE 9. Bond strengths (s in VU) on O atoms in PbF_L

	s(T-O)	s(Pb-O)	s(total)
OA(1)	1.71	0.41	2.12
OA(2)	1.74	0.39	2.13
OB(0)	1.83	0.15	1.98
OB(z)	1.90	0.06	1.96
OC(0)	1.85	0.04	1.89
OC(z)	1.84	0.09	1.93
OD(0)	1.80	0.16	1.96
OD(z)	1.73	0.27	2.00

balance, occupies (in PbF_H) a set of intermediate positions, related to local electrostatic configurations, and the shift away from the m plane can therefore assume larger values. This effect has not been observed in $C2/m$ strontium feldspar (obtained from melt) because the lack of a lone-pair effect renders Sr less sensitive to local charge imbalance.

An explanation in terms of dynamic disorder instead of static disorder seems less feasible because of the unusually large displacement factors of Pb in PbF_H at room temperature and by analogy with the current interpretation of Pb disorder in other Pb-bearing compounds (Downs et al. 1995). Clearly, the collection of in situ high-temperature single-crystal data is required to clarify the nature of this disorder.

DISCUSSION

The refinement of the PbF_L, annealed at T = 500 °C and P_{H_2O} = 2 kbar for 216 h, shows an almost ordered Al-Si configuration, which seems to represent the equilibrium state at low temperature. The Q_{od} value obtained from tetrahedral bond lengths is 0.89 for PbF_L (Table 5), close to that found in natural highly ordered anorthite (Q_{od} = 0.92, Angel et al. 1990). In contrast, crystals obtained from melt and cooled from T = 1280 to 1000 °C in 1 h and then to T = 700 °C in 15 h (PbF_H) have a completely disordered Al-Si configuration.

The results obtained show the presence of ordered and disordered configurations in the subsolidus region, in agreement with the suggestions made by Bruno and Fac-

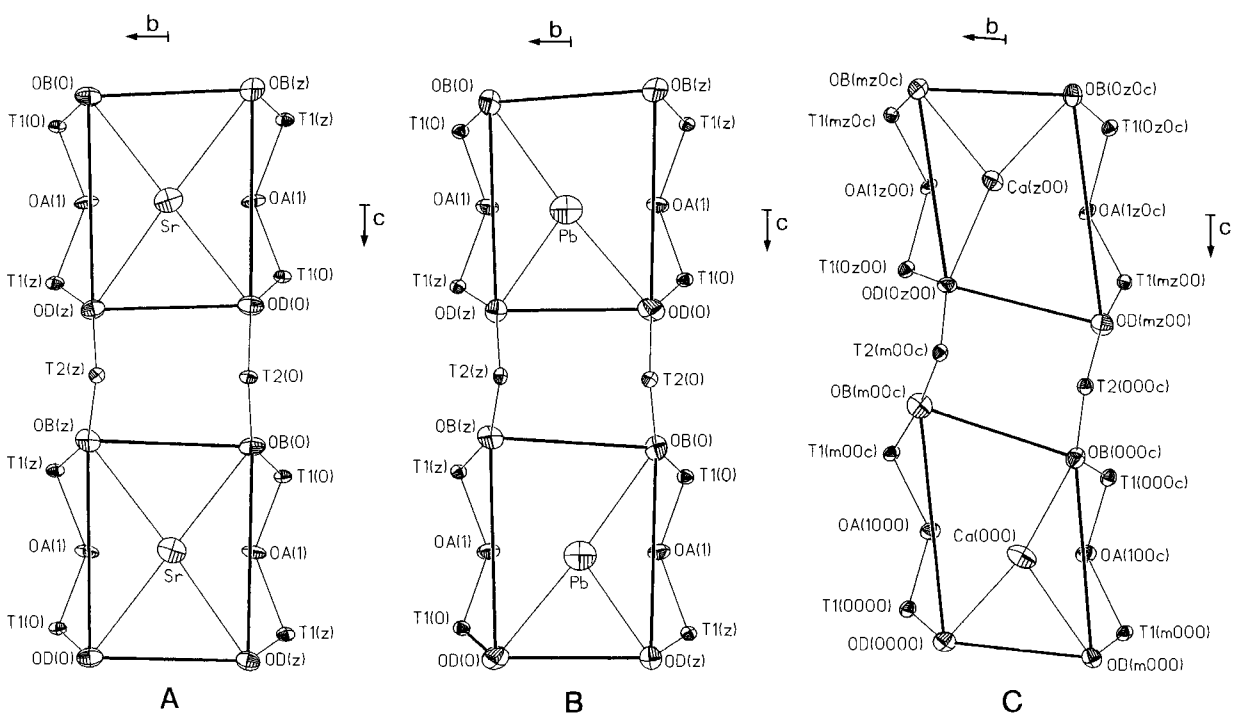

FIGURE 3. Partial coordination of the nontetrahedral cation. Projection on the (100) plane. (**A**) SrF, Benna et al. (1995) (T = 1350 °C, t = 678 h); (**B**) PbF_L, this work; (**C**) anorthite, Kalus (1978).

chinelli (1972). The possibility of obtaining a significant change in Al-Si configurations of lead feldspar at significantly shorter annealing times and lower temperatures than those required for alkaline-earth feldspars is also demonstrated. It still remains to be shown whether disordered Al-Si configurations are present in lead feldspar at equilibrium for temperatures close to $T_{solidus}$. However, faster reaction near $T_{solidus}$ should enable easier calibration of the Q_{od} evolution with temperature and time in the subsolidus region.

The cell parameters of PbF_H and PbF_L are significantly different, and in particular the *a* parameter seems to decrease with ordering. Similar behavior was observed in the order-disorder experiments of Bruno and Facchinelli (1972) and suggests the presence of a significant coelastic spontaneous strain resulting from Al-Si ordering. A significant change in the *a* parameter because of Al-Si ordering is anomalous in both alkali and alkaline-earth feldspars; on the other hand, *a* is significantly affected by the size of the nontetrahedral cation. This suggests a possible coupling between the Al-Si ordering and the distortion of the M-cation polyhedron.

Acknowledgments

We thank Simon A.T. Redfern for critical reading and useful suggestions. Reviews by Ross J. Angel and Martin D. McGuinn greatly improved the manuscript. This work was supported by Ministero della Ricerca Scientifica e Tecnologica and CNR, Rome.

References cited

Angel, R.J., Carpenter, M.A., and Finger, L.W. (1990) Structural variation associated with compositional variation and order-disorder behavior in anorthite-rich feldspars. American Mineralogist, 75, 150–162.

Benna, P., Zanini, G., and Bruno, E. (1985) Cell parameters of thermally treated anorthite. Al, Si configurations in the average structures of the high temperature calcic plagioclases. Contributions to Mineralogy and Petrology, 90, 381–385.

Benna, P., Tribaudino, M., and Bruno, E. (1995) Al-Si ordering in Sr-feldspar $SrAl_2Si_2O_8$: IR, TEM and single-crystal XRD evidences. Physics and Chemistry of Minerals, 22, 343–350.

Bown, M.G., and Gay, P. (1958) The reciprocal lattice geometry of the plagioclase feldspar structures. Zeitschrift für Kristallographie, 111, 1–14.

Brown, I.D., and Altermatt, D. (1985) Bond-valence parameters obtained from a systematic analysis of the inorganic crystal structure database. Acta Crystallographica, B41, 244–247.

Bruno, E., and Gazzoni, G. (1970) Feldspati sintetici della serie $Sr[Al_2Si_2O_8]$-$Pb[Al_2Si_2O_8]$. Periodico di Mineralogia, 39, 245–253.

Bruno, E., and Facchinelli, A. (1972) Al,Si configurations in lead feldspar. Zeitschrift für Kristallographie, 136, 296–304.

———(1974) Correlations between the unit-cell dimensions and the chemical and structural parameters in plagioclases and in alkaline-earth feldspars. Bulletin de la Société française de Minéralogie et de Cristallographie, 97, 378–385.

Bruno, E., Chiari, G., and Facchinelli, A. (1976) Anorthite quenched from 1530°C: I. Structure refinement. Acta Crystallographica, B32, 3270–3280.

Carpenter, M.A. (1991a) Mechanisms and kinetics of Al-Si ordering in anorthite: I. Incommensurate structure and domain coarsening. American Mineralogist, 76, 1110–1119.

———(1991b) Mechanisms and kinetics of Al-Si ordering in anorthite: II. Energetics and a Ginzburg-Landau rate law. American Mineralogist, 76, 1120–1133.

———(1992) Equilibrium thermodynamics of Al/Si ordering in anorthite. Physics and Chemistry of Minerals, 19, 1–24.

———(1994) Evolution and properties of antiphase boundaries in silicate minerals. Phase Transitions, 48, 189–199.

Carpenter, M.A., Angel, R.J., and Finger, L.W. (1990) Calibration of Al/Si order variations in anorthite. Contributions to Mineralogy and Petrology, 104, 471–480.

Chiari, G., Calleri, M., Bruno, E., and Ribbe, P.H. (1975) The structure of partially disordered, synthetic strontium feldspar. American Mineralogist, 60, 111–119.

Downs, R.T., Hazen, R.M., Finger, L.W., and Gasparik, T. (1995) Crystal chemistry of lead aluminosilicate hollandite: A new high-pressure synthetic phase with octahedral Si. American Mineralogist, 80, 937–940.

Griffen, D.T., and Ribbe, P.H. (1976) Refinement of the crystal structure of celsian. American Mineralogist, 61, 414–418.

Holtstam, D., Norrestam, R., and Sjödin, A. (1995) Plumboferrite: New mineralogical data and atomic arrangement. American Mineralogist, 80, 1065–1072.

Kalus, C. (1978) Neue Strukturbestimmung des Anorthits under Berücksichtigung möglicher Alternativen. Inaugural-Dissertation, Universität München, Munich, Germany.

Megaw, H.D. (1974) Tilts and tetrahedra in feldspars. In W.S. MacKenzie and J. Zussman, Eds., The feldspars, p. 87–113. Manchester University Press, Manchester, U.K.

Moore, P.B., Araki, T., and Ghose, S. (1982) Hyalotekite, a complex lead borosilicate: Its crystal structure and the lone-pair effect of Pb(II). American Mineralogist, 67, 1012–1020.

Moore, P.B., Sen Gupta, P.K., and Le Page, Y. (1989) Magnetoplumbite, $Pb^{2+}Fe^{3+}_{12}O_{19}$: Refinement and lone-pair splitting. American Mineralogist, 74, 1186–1194.

Moore, P.B., Sen Gupta, P.K., Shen, J., and Schlemper, E.O. (1991) The kentrolite-melanotekite series, $4Pb_2(Mn,Fe)^{3+}_2O_2[Si_2O_7]$: Chemical crystallographic relations, lone-pair splitting, and cation relation to 8URe,. American Mineralogist, 76, 1389–1399.

Moore, P.B., Davis, A.M., Van Derveer, D.G., and Sen Gupta, P.K. (1993) Joesmithite, a plumbous amphibole revisited and comments on bond valences. Mineralogy and Petrology, 48, 97–113.

Newnham, R.E., and Megaw, H.D. (1960) The crystal structure of celsian (barium feldspar). Acta Crystallographica, 13, 303–313.

North, A.C.T., Phillips, D.C., and Mathews, F.S. (1968) A semi-empirical method of absorption correction. Acta Crystallographica, A24, 351–359.

Phillips, B.L., Kirkpatrick, R.J., and Carpenter, M.A. (1992) Investigation of short-range Al,Si order in synthetic anorthite by ^{29}Si MAS NMR spectroscopy. American Mineralogist, 77, 484–494.

Shannon, R.D., and Prewitt, C.T. (1969) Effective ionic radii in oxides and fluorides. Acta Crystallographica, B25, 925–945.

Szymanski, J.T. (1988) The crystal structure of beudantite, $Pb(Fe,Al)_3[(As,S)O_4]_2(OH)_6$. Canadian Mineralogist, 26, 923–932.

Manuscript received January 8, 1996
Manuscript accepted June 26, 1996